

Alma Mater Studiorum Università di Bologna
Archivio istituzionale della ricerca

Synthesis, cytotoxicity and anti-cancer activity of new alkynyl-gold(I) complexes

This is the final peer-reviewed author's accepted manuscript (postprint) of the following publication:

Published Version:

De Nisi, A., Bergamini, C., Leonzio, M., Sartor, G., Fato, R., Naldi, M., et al. (2016). Synthesis, cytotoxicity and anti-cancer activity of new alkynyl-gold(I) complexes. DALTON TRANSACTIONS, 45, 1546-1553 [10.1039/c5dt02905h].

Availability:

This version is available at: <https://hdl.handle.net/11585/545974> since: 2022-02-14

Published:

DOI: <http://doi.org/10.1039/c5dt02905h>

Terms of use:

Some rights reserved. The terms and conditions for the reuse of this version of the manuscript are specified in the publishing policy. For all terms of use and more information see the publisher's website.

This item was downloaded from IRIS Università di Bologna (<https://cris.unibo.it/>).
When citing, please refer to the published version.

(Article begins on next page)

This is the final peer-reviewed accepted manuscript of:

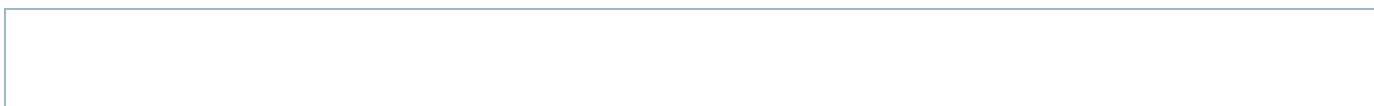
Synthesis, cytotoxicity and anti-cancer activity of new alkynyl-gold(i) complexes, Assunta

De Nisi, Christian Bergamini, Marco Leonzio, Giorgio Sartor, Romana Fato, Marina Naldi, Magda Monari,* Natalia Calonghi* and Marco Bandini*

The final published version is available online at: <https://doi.org/10.1039/C5DT02905H>

Rights / License:

The terms and conditions for the reuse of this version of the manuscript are specified in the publishing policy. For all terms of use and more information see the publisher's website.



alkynyl-gold(I) complexes

Synthesis, cytotoxicity and anti-cancer activity of new

Assunta De Nisi,^a Christian Bergamini,^b Marco Leonzio,^a Giorgio Sartor,^b Romana Fato,^b Marina Naldi,^b Magda Monari,^{*a} Natalia Calonghi^{*b} and Marco Bandini^{*a}

Alkynyl(triphenylphosphine)gold(I) complexes carrying variously substituted propargylic amines have been synthesized and fully characterized in solution and solid state. High levels of toxicity (*i.e.* micromolar range) were recognized for a series of cancer cell lines with particular emphasis on HT29, IGROV1, HL60 and I407. In particular the lead compound **3ab** was identified as the most active compound in all cell lines (IC_{50} : 1.7-7.9 μ M).

Introduction

The segment of metallodrugs based on gold complexes continues to gain credit within the scientific community due to their consolidated multiple pharmacological activities.¹ In particular, seminal discoveries focusing on the treatment of symptoms of rheumatoid arthritis² were expanded by applications of gold complexes as antimalaric agents³ and most recently also as anticancer drugs.⁴

The high toxicity that some gold(I), gold(III)⁵ and gold nanoparticles⁶/nanorods⁷ have shown against several tumour cell lines inspired the development of a number of structurally different organometallic species with chemical permutations both at the metal oxidation state and at the organic counterpart.⁸

In particular, the organic frameworks constituting the prodrug system proved to be actively involved in determining the overall toxicity of the species.⁹ In this direction, soft ligands such as phosphines, thiols (class-I polymeric thiolates, class-II monomeric thiolates)² or σ -donating nitrogen heterocyclic carbenes (NHCs)¹⁰ have been employed in gold complexes featuring anticancer activity.

Mechanistically, although the real target of gold-based organometallic species is still under debate, recent investigations unveiled that the observed cytotoxicity is mediated by their ability to alter mitochondrial functions through peculiar interactions with Se-containing enzymes TrxR.¹¹ This class of enzymes is involved in the defence against oxidative damage and in redox signalling. A growing number of transcription factors including NF- κ B or the Ref-1-dependent AP1 require thioredoxin reduction for DNA binding.¹² Moreover, recent studies have shown that the antiproliferative properties of gold(I) and gold(III) adducts may include their interaction with DNA: as a matter of fact, rapid inhibition of DNA synthesis was observed for gold(I) complexes containing AMPP, dppe or ADPP ligands.¹³

Very recently, Ott and coworkers documented on the synthesis, characterization and pharmacological investigation of a new family of mononuclear [alkynyl(triphenylphosphine)gold(I)] complexes of general structure $PPh_3Au-C\equiv CCH_2XR$ (X: O, N) with important antiproliferative activity (micromolar range) in breast adenocarcinoma and colon carcinoma cells.^{14a} Shortly after, the same team described the remarkable biological properties of binuclear gold(I) alkynyl analogous featuring bidentate phosphines as tethering units (Figure 1).^{14b} These works emphasized also thioredoxin reductase (TrxR)¹⁵ as a plausible biological target of pharmacologically active gold(I) species.¹⁶

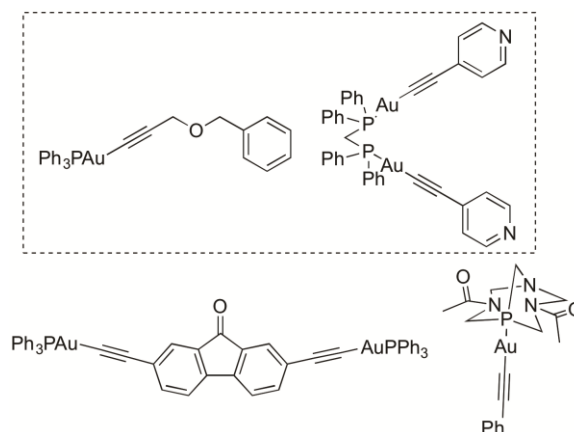


Figure 1. Collection of reported [alkynyl(phosphine)gold(I)] complexes featuring antitumor activity.

The propargylic sidearm proved to contribute substantially to the overall pharmacological activity of the titled species, therefore, careful modulation of this unit could lead to interesting perspectives in developing more selective and potent candidates for anticancer drugs.

In this regard, we present our recent investigation dealing with the documentation of novel [alkynyl(triphenylphosphine)gold(I)] complexes comprising relatively unexplored propargylic amine derivatives as organic ligands.^{14c} The possibility to create a chemical diversity by means of readily accessible propargylic amine derivatives enabled a survey of several structural aspects such as nitrogen basicity and electronic/steric factors.

Results and discussion

Synthesis and characterization

In order to assess the effective role of the alkynyl sidearm on the biological spectrum of the gold species, a range of propargylic mono- and diamine derivatives **2a-f** and mono/binuclear phosphinogold(I) complexes (*i.e.* PPh_3AuCl **1a** and $[PPh_2(CH_2)_2PPh_2](AuCl)_2$ **1b**)¹⁷, were elected as key building blocks (Chart 1).

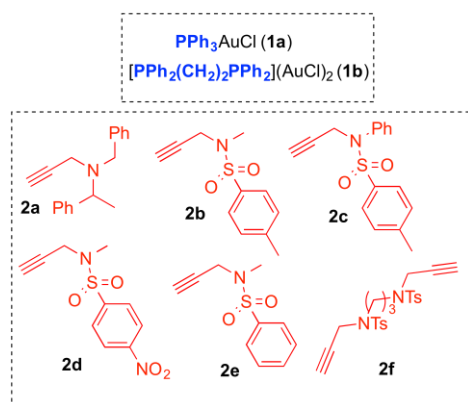
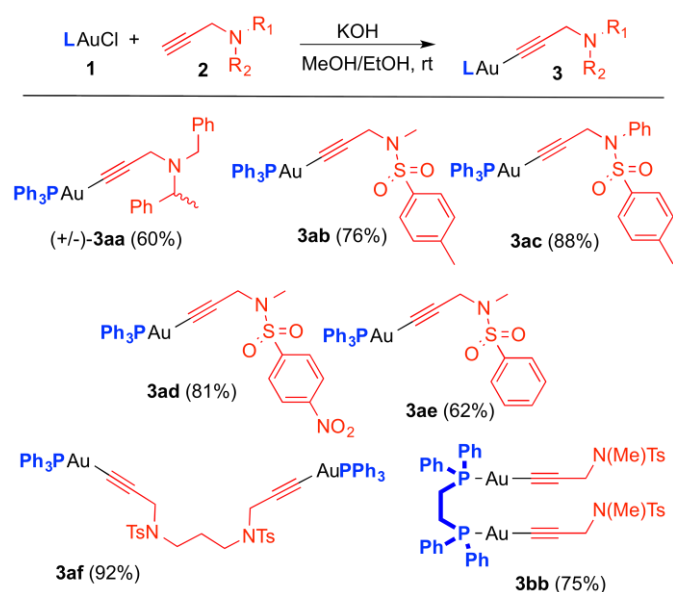


Chart 1. Metal and organic fragments employed in the present investigation.

In particular, by reacting an equimolar amount of gold(I)chloride complexes **1a,b** and the desired terminal alkyne under basic conditions (KOH, MeOH/EtOH), the corresponding alkynyl-gold complexes **3** were isolated in moderate to good yields (60-92%). Further purification was commonly carried out either by recrystallization or through flash chromatography on silica gel (Scheme 1).

Complexes **3** were obtained as white (pale brown in the case of **3ad**) air stable solids featuring a remarkable solubility in common organic solvents. They were fully characterized both in solution (NMR, IR, LC-MS) and solid state (**3ab** and **3ac**).

In particular, NMR spectroscopy (CDCl₃, rt) resulted particularly diagnostic in monitoring the reaction course. As a matter of fact, the formation of adducts **3** caused the disappearance of the acetylenic C-H of the alkyne congeners (¹H-NMR δ = 2.0-2.2 ppm), with the concomitant deshielding (≈ 0.15 ppm) of the propargylic methylene. Additionally, a marked downshielding of the ³¹P-NMR signals in the final compounds **3a-e** (39-42 ppm) occurred with respect to the congener **1a** (32.9 ppm). Contrarily, the ³¹P-NMR spectrum of the binuclear adduct **3bb** displayed a shielded singlet (δ = 21.8 ppm) if compared with **1b** (δ = 31.5 ppm). The presence of a single peak accounted for the formation of the C₂-symmetric adduct depicted in Scheme 1.



Scheme 1. Library of [gold(I)-alkynyl] complexes synthesized and tested in the present work. In brackets the isolated yields.

Solid state structure elucidation for complexes **3ab** and **3ac** was also carried out. In details, crystals suitable for X-ray diffraction were collected through slow evaporation of EtOAc solutions of the corresponding species and the resulting structures are reported in Figure 1.¹⁸ As expected for gold(I) complexes, Au adopts an almost linear coordination and the P-Au-C bond angles are very close to the ideal 180° [176.5(2) and 178.9(2)° for **3ab** and **3ac**, respectively]. The C≡C bond lengths of 1.183(7) and 1.194(7) Å are typical of terminal alkynyl gold(I) complexes. The crystal packing of **3ab** is dominated by weak non-classical intermolecular C-H...O hydrogen bonds whereas in **3ac** two phosphine phenyl rings in each molecule establish intermolecular π-π interactions with their symmetry equivalent adjacent phenyl ligands generating infinite zig-zag chains along the *c* axis (Figures S1 and S2).

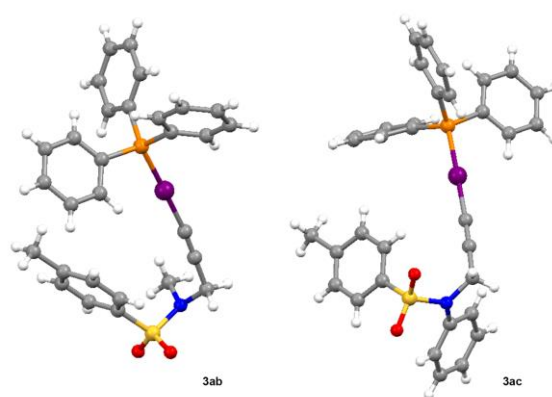


Figure 2. Molecular structure of **3ab** (left) and **3ac** (right).

Biology

Cell lines included in the evaluation of toxicity profiles were malignant HT29, IGROV1, and HL60, and a non-malignant human epithelial intestinal cell line I407. IC₅₀ values of the drugs were calculated using Prisma, fitted by means of sigmoidal fit and listed in Table 1.

Table 1. Half maximal Inhibitory Concentration (IC₅₀) of gold compounds in different cell lines after 24 h treatment (μM).^a

Compound	HT 29	IGROV 1	HL60	I407
Auranofin	3.3 (1.8-6)	2.5 (0.4-15)	0.7 (0.3-1.6)	1.6 (0.9-2.8)
(+/-)-3aa	> 100	20 (10.06-39.20)	19.0 (7.43-50.69)	15.0 (9.14-24.65)
3ab	7.9 (5.39-11.59)	5.3 (3.87-7.43)	3.3 (1.62-6.88)	1.7 (0.61-4.99)
3ac	> 100	5.5 (4.69-6.69)	2.7 (1.19-6.18)	9.6 (7.26-12.63)
3ad	11.0 (8.97-15.01)	6.5 (4.12-10.31)	6.3 (5.05-7.94)	8.0 (6.73-9.66)
3ae	> 100	10.0 (6.40-17.84)	9.0 (6.55-12.83)	> 100
3af	> 100	7.7 (6.26-9.48)	> 100	> 100
3bb	> 100	> 100	0.8 (0.28-2.40)	> 100

^a 95% confidence intervals are reported in brackets.

From the data collected in Table 1 some preliminary conclusions can be drawn. Within the portfolio of gold complexes in hand, **3ab** was the more effective in inhibiting cell growth in all panel cell lines, Auranofin, an antiarthritic gold(I) complex with antitumor activity, was included in the test panel for comparison^{19,20}. Additionally, also compound **3ad** showed some levels of cytotoxicity towards all the cell lines but the corresponding IC₅₀ values were constantly higher than that **3ab**. On the contrary, **(+/-)-3aa**, **3ac**, **3bb**, **3ae** and **3af** proved competent only on a few of the screened cell lines. In this scenario some peculiarities were also highlighted. In particular, complexes **3af** and **3bb** showed significant toxicity for IGROV1 and HL60 cells, respectively. Additionally, it is important to stress the lack of toxicity toward non-cancer cell lines showed by the compounds **3bb**, **3ae** and **3af**.

These bio-divergences clearly emphasised the role played by the presence of different moieties on the nitrogen atom in modulating the overall pharmacological properties of the gold complexes.

As mentioned above, inhibition of the seleno enzyme thioredoxin reductase (TrxR) is considered to be an important mechanism of bioactivity of gold(I) species²¹. In particular Auranofin shows an high inhibitory effect both on cytosolic (TrxR1) and mitochondrial (TrxR2) isoforms of this enzyme²². Therefore, the potential of gold complexes to inhibit TrxR was studied on commercially available TrxR using the 2,6-Dichloroindophenol (DCIP) reduction assay.

Table 2. Inhibition power of gold(I) complexes on TrxR in comparison with auranofin.^a

Compound	% of auranofin inhibition	IC ₅₀ (μM)
Auranofin	100	0.018
3bb	73	0.354
3af	73	0.308
3ae	52	1.555
3ad	55	3.754
3aa	33	0.818
3ab	--	--

^a First column: the inhibitory effect of different gold(I) complexes on TrxR is expressed as % of inhibition taking as reference the auranofin maximal inhibition. Second column: IC₅₀ values of the different gold(I) complexes and auranofin on TrxR activity.

According to the results given in Table 2, complexes **3bb** and **3af** turned out to be effective inhibitors of TrxR showing an inhibitory potency close to that induced by Auranofin and with IC₅₀ values in the sub-micromolar range. The other complexes showed IC₅₀ values at least two orders of magnitude higher than the auranofin. Whereas **3ab** cannot be considered an inhibitor of this class of enzymes.

It can be pointed out that only binuclear compounds are able to inhibit TrxR at sub-micromolar concentration suggesting a presence of strong interaction with the enzyme. To highlight the interaction between compounds and TrxR we have evaluated the LC-MS spectra of the enzyme both in the presence of a binuclear compound (**3bb**) and in the presence of the mononuclear compound **3ab** that does not inhibit the enzyme activity.

The results, reported in the supplementary section, indicate that no covalent bond exists between TrxR and **3ab** or **3bb** (Figure S3 and Figure S4).

To gain some insights into the biological effects of these new derivatives, the most active compound toward all cells lines, **3ab** was submitted to additional studies. In order to assess whether its effect was due to interference with cell cycle progression, DNA profiles of cultured cells were examined by flow cytometry and cell cycle analysis was performed by using the Multicycle Cycle Phoenix Flow system, and Modfit 5.0 software. Table 3 shows that the treatment with **3ab** caused a marked accumulation of HT29, IGROV1 and I407 cells in the S phase, with respect to untreated cells.

Table 3. Cell cycle distribution of cell lines treated with **3ab**.^a

	G0/G1 %	S %	G2/M %
HT29	49,05	39,58	11,37
HT29 + 3ab (7.9 μM)	45,72	45,25	9,03
IGROV1	55,32	29,57	15,11
IGROV1 + 3ab (5.3 μM)	50,71	37,16	12,13
I407	70,38	23,62	6
I407 + 3ab (1.7 μM)	62,64	28,52	8,84

Contrarily, in HL60 treated cells, the growth arrest was in the G0/G1 phase of the cell cycle was associated with a well distinguishable pre-G1 peak in DNA, suggestive of DNA fragmentation, characteristic of apoptosis (Figure 3).

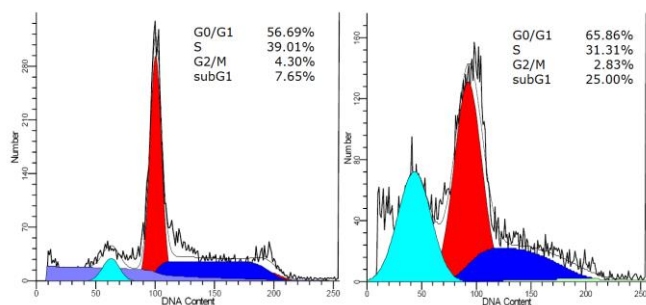


Figure 3. Effect of compound **3ab** on HL60 cell cycle. Cells were incubated for 24 h, (sx) with the vehicle (Ctrl), or (dx) with compound **3ab** (3.3 μ M), afterward cell cycle distribution was determined by flow cytometry. Following treatment with **3ab**, cells are in the G0/G1 phase and a well detectable fraction of DNA is present as a sub-G1 peak (light blue peak).

Interestingly, the treatment with the binuclear compounds did not induce any effect on cell cycle, as reported in Table 4, where the cell cycle distribution of IGROV1 and HL60 in the presence of **3af** and **3bb**, respectively is shown.

Table 4. Cell cycle distribution of cell lines treated with **3af** and **3bb**.^a

	G0/G1 %	S %	G2/M %
IGROV1	60	25	15
IGROV1 + 3af (7.7 μ M)	64	23	13
HL60	48	14	38
HL60 + 3bb (0.8 μ M)	50	17	33

UV-Vis absorption titration analysis

Interactions between small molecules and DNA rank among the primary action mechanisms of cytotoxic activity. In order to compare the binding properties of the gold complexes with DNA, dissociation constants (K_d) were determined through inverse titration experiments. Two types of interactions can be devised by these experiments as we can argue by the either an increase or a decrease of ΔA measured at 260 nm.

The increase of differential absorption of DNA in the presence of **3af**, **3ab**, **3ac**, **3bb**, and **3ad** can be ascribed to a lower base stacking while the decreased differential absorbance observed for (+/-)-**3aa** suggests a higher compactness of DNA. No appreciable effect was observed for **3ad**. In this regard, the differential spectra of **3af** (A), (+/-)-**3aa** (B) and **3ad** (C) are depicted in Figure 4.

We then plot the differential absorbance at 260 nm for each molecule versus DNA concentration, as reported in Figure 5.

The estimation of the dissociation constant (K_d) for the complex formation as well as the limiting value for the ΔA_{260} was obtained fitting these data using a one-site saturation equation (Table 5).

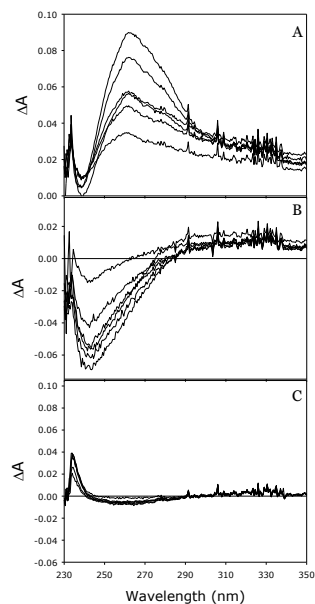


Figure 4. Differential absorption spectra of **3af** (A), (+/-)-**3aa** (B) and **3ad** (C) titrated with DNA.

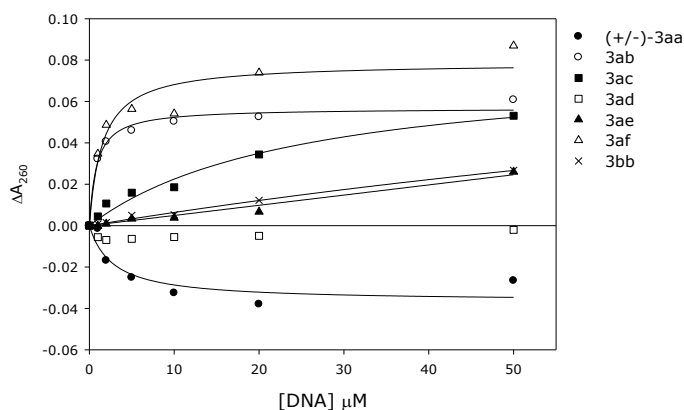


Figure 5. Differential absorbance at 260 nm of DNA-Molecule complexes at increasing DNA concentration. Molecule concentration was 10 μ M.

Table 5. Dissociation constant for the complex formation and the limiting value for the ΔA_{260} obtained by fitting data in Figure 5.

Compound	$K_d \pm SE$ (μ M)	$B_{max} \pm SE$	r^2
(+/-)- 3aa	2.78 ± 1.63	-0.0366 ± 0.0055	0.8564
3ab	0.84 ± 0.17	0.0568 ± 0.0019	0.9826
3ac	24.89 ± 7.12	0.0784 ± 0.0108	0.9757
3bb	195.53 ± 111.89	0.1310 ± 0.0619	0.9923
3ad	--	--	--
3ac	--	--	--
3af	1.54 ± 0.58	0.0786 ± 0.0064	0.9245

The K_d analysis confirms that **3ab** interacts with DNA quite strongly ($K_d = 0.84 \pm 0.17$ μ M) suggesting a partial explanation for its cellular toxicity. Among the other compounds, only **3af** shows a strong interaction with DNA having a similar value of K_d (1.54 ± 0.58 μ M). On the other hand, a decrease for the differential absorbance

spectra is observed for (+/-)-**3aa**. While the increase in the absorbance at 260 nm can be ascribed to a partial DNA denaturation, the decrease observed in the presence of the compound **3aa**, could be indicative of DNA supercoiling.

Fluorescence titration of 15 μM ETBr bound to DNA with **3ab**, up to 200 μM , does not show any appreciable change of the emission spectra of ETBr, suggesting that no intercalation of **3ab** with DNA takes place (Figure 6).

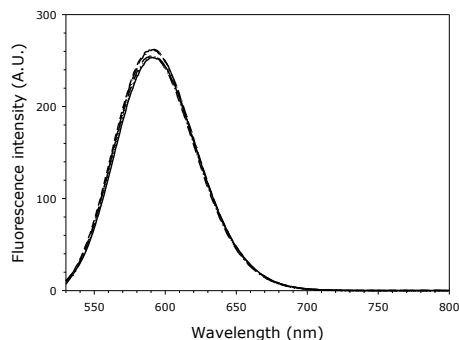


Figure 6 Fluorescence emission spectra of 15 μM ETBr bound to DNA in presence of increasing concentration of **3ab**. Control: solid line; [**3ab**] 10 μM : long dashed line; [**3ab**] 50 μM : short dashed line; [**3ab**] 100 μM : dashed dotted line; [**3ab**] 200 μM : dotted line.

Conclusions

In conclusion, a new class of neutral [Au(I)]-alkynyl complexes based on monodentate or bidentate phosphine ligands has been developed and fully characterized both at the liquid and solid state. The gold(I)-C_{sp} linkage was efficiently realized in high yields (60–92%) by condensing the gold-chloride congener with pre-functionalized terminal alkynes under convenient mild conditions (KOH, MeOH/EtOH).

Additionally, the biological activity of these organometallic species was comprehensively investigated and the data reported suggest that their cellular toxicity could be related to different mechanisms acting on different biological targets.

Compound **3ab** showed a marked cytotoxicity on all cell lines tested, with IC₅₀ values comprised from 1.7 μM for I407 to 7.9 μM for HT29 and caused cell cycle arrest in the S phase. Only in HL60 cell line the growth arrest was in the G0/G1 phase of the cell cycle and it was associated with a well distinguishable pre-G1 peak that indicates DNA fragmentation that is characteristic of apoptosis. These effects on cell cycle can be associated to an interaction of the molecule with DNA and this hypothesis is supported by the results of DNA titration where the dissociation constant of **3ab** with salmon sperm DNA is in the sub-micromolar range. The real mechanism of **3ab**-DNA interaction has yet not been fully elucidated, however, it cannot be attributed to an intercalation of the molecule into DNA helix. Additionally, It should be mentioned that **3ab** does not show any inhibitory effect on the thioredoxin reductase enzymatic activity.

On the other hand, the binuclear compounds (**3bb** and **3af**) showed a cytotoxic effect only in HL60 (**3bb**: IC₅₀ = 0.8 μM) and in IGROV1 (**3af**: IC₅₀ = 7.7 μM) and they do not showed any effect on cell cycle (Table 4). This evidence suggests that the biological target of binuclear gold-species is not the DNA and they appear to act through the inhibition of thioredoxin reductase at sub-micromolar concentration (Table 2). However the mechanism of

interaction of our alkynyl-gold(I) complexes with thioredoxin reductase is different as compared to Auranofin and other gold compounds.²³ In fact, while Auranofin induces a mass shift in the mass spectra of this enzyme suggestive of protein binding of the gold-containing molecule²², In our study no covalent adducts with the enzyme have been detected using LC/ESI-MS (see SI).

Moreover, inhibition of thioredoxin reductase is responsible for a decrease of the oxidative stress resistance and for alterations in redox signalling that are key factors for cell survival. Being cancer cells more resistant toward oxidative stress, these compounds, that are able to interfere with these phenomena, have a good chance to be candidate as anticancer drugs. Studies addressing the clarification and/or identification of additional biological targets as well as the development of structure–activity relationships are currently on going in our laboratories.

Acknowledgements

Acknowledgements for funding are made to MIUR – Rome - and University of Bologna. We are also grateful to Si Hui Elisa Chen and Ciro Romano for the technical assistance and helpful discussion.

Experimental

Synthesis of the nitrogen containing [alkynylAu(I)] complexes **3**

A solution of desired alkyne (1.2 or 2.4 eq.) in reagent grade MeOH/EtOH (1:1 ratio, 0.05 M) was treated with the desired gold(I)chloride precursor (**1a,b**, 1 eq.) and a solution of KOH (4 eq., 2 M in MeOH). The mixture was stirred under dark until complete consumption of the alkyne. The resulting solid was collected by filtration and washed with cooled MeOH. Pure material can be obtained via re-crystallization from a DCM:pentane solution, or flash chromatography.

(+/-)-**3aa**: white solid, purification via flash chromatography (cHex:AcOEt = 9:1-7:3); yield = 60%; °C; IR = 2159 cm⁻¹ (C≡C); ¹H-NMR (400 MHz, CDCl₃): δ 1.44 (d, J(H,H) = 6.4 Hz, 3H); 3.40 (d, J(H,H) = 17.6 Hz, 1H); 3.61 (d, J(H,H) = 2.0 Hz, 2H); 3.68 (d, J(H,H) = 17.6 Hz, 1H); 4.00 (q, J(H,H) = 6.4 Hz, 1H); 7.24-7.52 (m, 25H); ¹³C-NMR (100 MHz, CDCl₃): δ 21.4, 39.5, 54.3, 60.5, 98.0, 98.2, 124.3, 126.5, 126.6, 126.9, 127.6, 128.0, 128.2, 128.4, 128.9, 129.0, 129.1, 129.7, 130.2, 131.5, 132.5, 134.3, 134.4, 140.2, 146.2; ³¹P-NMR (162 MHz, CDCl₃): δ = 42.0 (br s) ppm; ESI Q-TOF for (C₃₆H₃₃AuNP: 707.2016), (m/z): 708.2090 (M+H⁺).

3ab: white solid; yield = 76%; Mp = 175-177 °C; IR = 2137 cm⁻¹ (C≡C); ¹H-NMR (400 MHz, CDCl₃): δ = 2.29 (s, 3H); 2.86 (s, 3H); 4.08 (s, 2H); 7.25 (d, J(H,H) = 7.2 Hz, 2H); 7.44 (m, 15H); 7.73 (d, J(H,H) = 7.2 Hz, 2H); ¹³C-NMR (100 MHz, CDCl₃, diagnostic signals): δ = 21.4, 34.2, 41.0, 95.4, 95.6, 128.1, 129.1, 129.2, 129.4, 129.9, 131.6, 134.2, 134.3, 143.1; ³¹P-NMR (162 MHz, CDCl₃): δ = 41.9 (br s) ppm; LC/MS-ESI (m/z): ESI Q-TOF for (C₂₉H₂₇AuNO₂PS: 681.1196), (m/z): 682.1244 (M+H⁺).

3ac: white solid; yield = 88%; Mp = 139-141 °C; IR = 2134 cm⁻¹ (C≡C); ¹H-NMR (400 MHz, CDCl₃): δ = 2.32 (brs, 3H); 4.61 (s, 2H); 7.17 (d, J(H,H) = 8.4 Hz, 2H); 7.26-7.35 (m, 2H); 7.37-7.38 (m, 2H); 7.44-7.54 (m, 16H); 7.64 (d, J(H,H) = 8.4 Hz, 2H); ¹³C-NMR (100 MHz, CDCl₃, diagnostic signals): δ = 21.5, 42.2, 127.4, 128.2, 128.3, 128.8, 129.0, 129.1, 129.2, 130.0, 131.6, 134.2, 134.3, 136.0, 140.0, 142.9; ³¹P-NMR (162 MHz, CDCl₃): δ = 42.4 (s) ppm;

ESI Q-TOF for (C₃₄H₂₉AuNO₂PS: 743.1322), (m/z): 766.1220 (M+Na⁺).

3ad: pale yellow solid; yield = 81%; Mp = 208-210 °C; IR = 2137 cm⁻¹ (C≡C); ¹H-NMR (400 MHz, CDCl₃): δ = 2.95 (s, 3H); 4.27 (d, J(H,H) = 1.6 Hz, 2H); 7.43-7.53 (m, 15H); 8.13 (d, J(H,H) = 8.8 Hz, 2H); 8.34 (d, J(H,H) = 8.8 Hz, 2H); ¹³C-NMR (100 MHz, CDCl₃): δ = 34.4, 41.2, 93.7, 94.0, 123.9, 129.2, 129.6, 131.6, 134.0, 134.2, 143.8, 149.9; ³¹P-NMR (162 MHz, CDCl₃): δ = 39.4 (s) ppm; ESI Q-TOF for (C₂₈H₂₄AuN₂O₂PS: 712.0860), (m/z): 713.0940 (M+H⁺).

3ae: white solid; yield = 62%; Mp = 210-212 °C; IR = 2136 cm⁻¹ (C≡C); ¹H-NMR (400 MHz, CDCl₃): δ = 2.91 (s, 3H); 4.14 (s, 2H); 7.44-7.48 (m, 18H); 7.88 (d, J(H,H) = 6.8 Hz, 2H); ¹³C-NMR (100 MHz, CDCl₃, diagnostic signals): δ = 34.3, 41.0, 95.3, 99.0, 127.8, 128.1, 128.7, 129.0, 129.1, 129.2, 129.4, 129.9, 131.6, 131.7, 132.4, 134.1, 134.3, 137.5; ³¹P-NMR (162 MHz, CDCl₃): δ = 39.2 (s) ppm; ESI Q-TOF for (C₂₈H₂₅AuNO₂PS: 667.1009), (m/z): 668.1088 (M+H⁺).

3af: pale yellow solid; yield = 92%; Mp = decomposition; IR = 2132 cm⁻¹ (C≡C); ¹H-NMR (400 MHz, CDCl₃): δ = 1.97-1.98 (m, 2H), 2.24 (s, 6H), 3.37 (t, J(H,H) = 6.8 Hz, 4H), 4.29 (s, 4H), 7.22-7.29 (d, J(H,H) = 8.4 Hz, 4H), 7.45-7.56 (m, 30H), 7.81 (d, J(H,H) = 8.4 Hz, 4H); ¹³C-NMR (100 MHz, CDCl₃, diagnostic signals): δ = 21.4, 25.8, 37.6, 43.7, 95.1, 127.7, 127.8, 127.9, 129.0, 129.1, 129.2, 129.4, 130.0, 131.4, 131.5, 134.1, 134.2, 136.1, 142.7; ³¹P-NMR (162 MHz, CDCl₃): δ = 40.9 (br s); LC/MS-ESI (m/z): 1375 (M+H⁺).

3bb: white solid; yield = 75%; IR = 2123 cm⁻¹ (C≡C); ¹H-NMR (400 MHz, CDCl₃): δ = 1.70 (s, 1H), 2.31 (s, 6H); 2.86 (s, 6H); 4.05 (s, 4H); 7.26-7.72 (m, 30H); ¹³C-NMR (100 MHz, CD₃CN, diagnostic signals): δ = 20.6, 33.5, 33.9, 40.9, 41.4, 77.6, 92.4, 127.8, 127.9, 128.9, 129.4, 129.5, 129.6, 130.4, 131.9, 132.2, 133.3, 133.4, 143.6; ³¹P-NMR (162 MHz, CDCl₃): δ = 21.8 ppm.

Cell culture and cytotoxicity

Cell lines (HT29, IGROV1, HL60 and I407) were routinely cultured in RPMI 1640 medium (Lonza) supplemented with penicillin (Sigma-Aldrich) (100 U/mL), streptomycin (Sigma-Aldrich) (100 µg/mL), and 10% fetal bovine serum (Euroclone) in an environment of 5% CO₂, 37 °C and sub-cultured using a trypsin 0.25%-EDTA (Sigma-Aldrich) 0.02% solution. The cytotoxicity was determined with the MTT (3-(4,5-dimethylthiazol-2-yl)-2,5-diphenyltetrazolium bromide) (Sigma-Aldrich) dye reduction assay.

Cells were plated in 96-well flat-bottomed microplates at a density of 1 × 10⁵ cells/mL (100 µL/well), and 24 h later the test compounds were added, appropriately diluted with DMSO. Cells were exposed to various concentrations of the compounds (in a range 1 nM to 100 µM) for 24 h. The cytotoxicity was determined with the MTT (3-(4,5-dimethylthiazol-2-yl)-2,5-diphenyltetrazolium bromide) dye reduction assay with minor modifications.^[20] Briefly, after incubation with the test compounds, MTT solution (0,2 mg/mL in PBS) was added (100 µL/well). Plates were further incubated for 2 h at 37 °C, and the formazan crystals formed were dissolved by adding 100 µL/well of propanol. Optical densitometry was determined with a Wallac 1420 Victor2 Microplate Reader (Perkin Elmer) at 570 nm.

One hundred microliters of culture medium supplemented with the same amount of MTT solution and solvent was used as blank solution. The IC₅₀ value was calculated according to the GraphPad Prism GraphPad Prism 5 software. All data are expressed as mean ± SD.

Cell cycle analysis

Cells were plated at initial density of 10000-20000 cell/cm² in dish or flask, depended on the cell line. After 72 h of adhesion, cells were treated with drugs at the concentration correspond to the calculated IC₅₀, and after 24 h of treatment the effect was evaluated. Untreated and 24 h treated cells were detached, washed in PBS and the pellet was finally re-suspended in 0.01% Nonidet P-40 (Sigma-Aldrich), 10 µg/mL RNase (Sigma-Aldrich), 0.1% sodium citrate (Sigma-Aldrich), 50 µg/mL propidium iodide (PI) (Sigma-Aldrich), for 30 min at room temperature in the dark. Propidium iodide (PI) fluorescence was analyzed using a Beckman Coulter Epics XL-MCL flow cytometer and cell analysis was performed using the M cycle (Verity) and MODFIT 5.0 softwares.

TrxR inhibition assay

For this purpose, commercially available rat liver TrxR (Sigma-Aldrich) was used and diluted with distilled water to achieve a concentration of 0.05 U mL⁻¹. The gold(I) complexes were freshly dissolved as stock solutions in DMSO. The reduction of the DCIP (2,6-Dichloroindophenol) was followed spectrophotometrically at 600nm using ε=19,1mM cm⁻¹ using a Jasco V-550 spectrophotometer equipped with stirring device and thermostatic control.

To each cuvette was added: 100 µL of enzyme solution, different concentrations of the compounds (ranging from 1 to 100 µM) or vehicle, 100 µM DCIP, 8 mM EDTA, 0,001% BSA in 20 mM potassium phosphate buffer pH 7,1 ml final volume.

The reaction was started by the addition of 2mM NADPH. The IC₅₀ values were calculated as the concentration of compound required to decrease enzyme activity of the untreated control by 50%, and are given as the means ± SD of 3–6 independent experiments.

DNA-compound interaction assay

The absorbance spectra were obtained scanning the solution in 1 cm quartz cuvettes from 230 nm to 400 nm using a (band width 2 nm). The solubility of different compounds was checked evaluating the lack of scattering. Then additions standard DNA was performed. After each addition of DNA the absorbance spectrum was recorded. The DNA stock solution was prepared with low molecular weight from salmon sperm, Sigma Aldrich in BS. The DNA stock solution concentration was determined spectrophotometrically (λ: 260 nm), using an extinction coefficient of 6600 M⁻¹ cm⁻¹.

The blank were prepared with standard DNA titration from 1 µM to 50 µM in BS and 4% of DMSO.

The UV-Vis spectra of DNA in the presence of the different compounds were obtained using a Jasco v-550 spectrophotometer (see SI). The data analysis was carried out on the subtracted spectrum (ΔA_λ): the spectra of titration experiments were subtracted by standard DNA titration and compound lacking DNA.

$$\Delta A_{\lambda} = (\Delta A_{\text{DNA-compound}})_{\lambda} - (\Delta A_{\text{DNA}})_{\lambda} - (\Delta A_{\text{compound}})_{\lambda}$$

The compounds absorbance variations at 260 nm (ΔA₂₆₀) were plotted versus DNA concentration. The calculation of binding parameters was carried out fitting ΔA₂₆₀ using following equation:

$$\Delta A_{260} = \frac{B_{\text{max}}[\text{DNA}]}{K_d + [\text{DNA}]}$$

Where K_d represents the dissociated constant of DNA complex for every compound and B_{max} represents the limiting value of ΔA_{260} .

Competitive Binding Fluorescence Studies

Aliquots of stock solution of the gold complex **3ab** dissolved in DMSO were added to solutions containing 15 μ M calf thymus DNA (ctDNA) base pairs and 15 μ M ethidium bromide (ETBr) in 15% DMSO 25 mM Tris-HCl buffer (pH 7.0) at 25 °C to give final complex concentration ranging from 0 to 200 μ M, according to the litreure.²² Excitation wavelength was set at 500 nm and emission spectra were recorded between 530 and 800 nm. Blanck subtraction was applied.

Notes and references

† CCDC 1045016 (**3ab**), CCDC 1045017 (**3ac**) contain the supplementary crystallographic data for this paper. These data can be obtained free of charge from the Cambridge Crystallographic Data Centre via www.ccdc.cam.ac.uk/data_request/cif.

- 1 For a collection of recent reviews see: a) C. F. Shaw III, *Chem. Rev.* 1999, **99**, 2589-2600; b) P. J. Barnard, S. J. Berners-Price *Coord. Chem. Rev.* 2007, **251**, 1889-1902; c) I. Ott *Coord. Chem. Rev.* 2009, **253**, 1670-1681; d) S. Nobili, E. Mini, I. Landini, C. Gabbiani, A. Casini, L. Messori, *Med. Res. Rev.* 2010, **30**, 550-580; e) S. J. Tan, Y. K. Yan, P. P. F. Lee, K. H. Lim, *Future Med. Chem.* 2010, **2**, 1591-1608; f) S. J. Berners-Price in *Bioinorganic Medicinal Chemistry* (Ed. E. Alessio), Weinheim, 2011; g) S. Komeda, A. Casini, *Curr. Top. Med. Chem.* 2012, **12**, 219-235. h) K. D. Mjos, C. Orvig, *Chem. Rev.* 2014, **114**, 4540-4563.
- 2 The most recently introduced gold(I)-drug for treatment of the symptoms of rheumatoid arthritis is auranofin (commercial name Ridaura®) in the 1985: a) B. M. Sutton, E. McGusty, D. T. Walz, M. J. DiMartino, *J. Med. Chem.* 1972, **15**, 1095-1098; b) B. M. Sutton, *Bull. Gold* 1986, **19**, 15-16.
- 3 For recent publications on the field see: a) M. Altaf, M. Monim-ul-Mehboob, A. A. Seliman, M. Sohail, M. I. M. Wazeer, A. A. Isab, L. Li, V. Dhuna, G. Bhatia, K. Dhuna, *Eur. J. Med. Chem.* 2015, **90**, 464-472; b) L. Boselli, M. Carraz, S. Mazeret, L. Paloque, G. Gonzalez, F. Benoit-Vical, A. Valentin, C. Hemmert, H. Gornitzka, *Organometallics*, 2015, **34**, 1046-1055; c) N. Pantelic, T. P. Stanojkovic, B. B. Zmejovski, T. J. Sabo, G. N. Kaluderovic, *Eur. J. Med. Chem.* 2015, **90**, 766-774; d) T. Traut-Johnstone, S. Kanyanda, F. H. Kriel, T. Viljoen, P. D. R. Kotze, W. E. van Zyl, J. Coates, D. J. G. Rees, M. Meyer, R. Hewer, D. Bradley G. Williams, *J. Inorg. Biochem.* 2015, **145**, 108-120.
- 4 M. Navarro, *Coord. Chem. Rev.* 2009, **253**, 1619-1626. b) J. Coetzee, S. Cronje, L. Dobrzanska, H. G. Raubenheimer, G. Joone, M. J. Nell, H. C. Hoppe, *Dalton Trans.*, 2011, **40**, 1471-1483.
- 5 For representative examples: a) P. I. da Silva Maia, V. M. Deflon, U. Abram, *Future Med. Chem.* 2014, **6**, 1515-1536; b) C. T. Lum, R. W.-Y. Sun, T. Zou, C.-M. Che, *Chem. Sci.* 2014, **5**, 1579-1584.
- 6 a) B. Kang, M. A. Mackey, M. A. El-Sayed, *J. Am. Chem. Soc.* 2010, **132**, 1517-1519; b) R. Geetha, T. Ashokkumar, S. Tamilselvan, K. Govindaraju, M. Sadiq, G. Singaravelu, *Cancer Nanotechnology*, 2013, **4**, 91-98 c) C. C. Chen, D. S. Hsieh, K. J. Huang, Y. L. Chan, P. D. Hong, M. K. Yeh, C. J. Wu, *Drug Design*, 2014, **16**, 459-474; d) U. Y. Lee, Y. S. Youn, J. Park, E. S. Lee, *ACS Nano*, 2014, **8**, 12858-12865.
- 7 R. Mooney, L. Roma, D. Zhao, D. Van Haute, E. Garcia, S. U. Kim, A. J. Annala, K. S. Aboody, J. M. Berlin, *ACS Nano*, 2014, **8**, 12450-12460.
- 8 C. Nardon, G. Boscutti, D. Fregona, *Anticancer Res.*, 2014, **34**, 487-492.
- 9 S. J. Berners-Price, P. J. Barnard, in *Ligand Design in Medicinal Inorganic Chemistry*, Wiley, 2014, pp. 227-256.
- 10 a) L. Messori, C. Gabbiani, *Metals Compounds in Cancer Chemotherapy* (Eds. J. M. Pérez, M. A. Fuertes, C. Alonso). Research Signpost, 2005, 355-375; b) S. Pengfei, J. Qin, *Progress in Chemistry*, 2009, **21**, 644-653; c) Tessier, C. L. Cannon, W. J. Youngs, *Chem. Rev.* 2009, **109**, 3859-3884; d) R. Rubbiani, S. Can, I. Kitanovic, H. Alborzina, M. Stefanopoulou, M. Kokoschka, S. Mönchgesang, W. S. Sheldrick, S. Wölfl, I. Ott, *J. Med. Chem.* 2011, **54**, 8646-8657; e) W. Liu, R. Gust, *Chem. Soc. Rev.* 2013, **42**, 755-773; f) F. Cisnetti, A. Gautier, *Angew. Chem. Int. Ed.* 2013, **52**, 11976-11978; g) C. Hu, X. Li, W. Wang, R. Zhang, L. Deng, *Curr. Med. Chem.* 2014, **21**, 1220-1230; h) X. Cheng, P. Holenya, S. Can, H. Alborzina, T. Rubbiani, I. Ott, S. Woelfl, Stefan, *Mol. Cancer*, 2014, **13**, 221/1-221/15; i) M. Tacke, *J. Organomet. Chem.* 2015, **782**, 17-21; h) E. Garcia-Moreno, S. Gascon, J. A. Garcia de Jalon, E. Romanos, M. J. Rodriguez-Yoldi, M. Laguna, *Anti-Cancer Agents Med. Chem.*, 2015, **10**, 773-782
- 11 a) I. Ott, *Coord. Chem. Rev.* 2009, **253**, 1670-1681; b) P. J. Barnard, S. J. Berners-Price, *Coord. Chem. Rev.* 2007, **251**, 1889-1902; c) C. Marzano, V. Gandin, A. Folda, G. Scutari, A. Bindoli, M. P. Rigobello, *Free Rad. Biol. Med.* 2008, **42**, 872-881; d) V. Gandin, A. P. Fernandes, M. P. Rigobello, B. Dani, F. Sorrentino, F. Tisato, M. Björnstedt, A. Bindoli, A. Sturaro, R. Rella, C. Marzano, *Biochem Pharmacol.* 2010, **15**, 90-101; e) T. V. Serebryanskaya, A. S. Lyakhov, L. S. Ivashkevich, J. Schur, C. Frias, A. Prokop, I. Ott, *Dalton Transactions* 2015, **44**, 1161-1169.
- 12 a) E. S. Arner, A. Holmgren, *Eur. J. Biochem.* 2000, **267**, 6102-6109; b) L. Ortego, F. Cardoso, S. Martins, M. F. Fillat, A. Laguna, M. Meireles, M. D. Villacampa, M. C. Gimeno, *J. Inorg. Biochem.* 2014, **130**, 32-37.
- 13 a) S. J. Berners-Price, C. K. Mirabelli, R. K. Johnson, M. R. Mattern, F. L. McCabe, L. F. Faucette, C. M. Sung, S. M. Mong, P. J. Sadler, S. T. Crooke, *Cancer Res.*, 1986, **46**, 5486-5493; b) M. J. McKeage, P. Papatheanasiou, G. Salem, A. Sjaarda, G. F. Swiegers, P. Waring, S. B. Wild, *Metal-Based Drugs*, 1998, **5**, 217-223; c) G. Lupidi, L. Avenali, M. Bramucci, L. Quassinti, R. Pettinari, H. K. Khalife, H. Gali-Muhtasib, F. Marchetti, C. Pettinari, *J. Inorg. Biochem.*, 2013, **124**, 78-87; d) F. Kuralay, A. Erdem, *Analyst*, 2015, **140**, 2876-2880.
- 14 a) A. Meyer, C. P. Bagowski, M. Kokoschka, M. Stefanopoulou, H. Alborzina, S. Can, D. H. Vlecken, W. S. Sheldrick, S. Wölfl, I. Ott, *Angew. Chem.* 2012, **124**, 9025-9030; *Angew. Chem. Int. Ed.* 2012, **51**, 8895-8899; b) A. Meyer, A. Gutiérrez, I. Ott, L. Rodríguez, *Inorg. Chim. Acta*, 2013, **398**, 72-76.
- 15 See also: a) E. Schuh, S. M. Validi, M. A. Jakupec, B. K. Keppler, P. Chiba, F. Mohr, *Dalton Trans.* 2009, 10841-10845; b) C. H. Chiu, R. S. M. Wong, R. Gambari, G. Y. M. Cheng, M. C. W. Yuen, K. W. Chan, S. W. Tong, F. Y. Lau, P. B. S. Lai, K. H. Lam, C. L. Ho, C. W. Kan, K. S. Y. Leung, W. Y. Wong, *Bioorg. Med. Chem.* 2009, **17**, 7872-7877; c) E. Vergara, E. Cerrada, A. Casini, O. Zava, M. Laguna, P. J. Dyson, *Organometallics* 2010, **29**, 2596-2603; d) R. G. Balasingham, C. F. Williams, H. J. Mottram, M. P. Coogan, S. J. A. Pope, *Organometallics* 2012, **31**, 5835-5843.
- 16 a) A. Bindoli, M. P. Rigobello, G. Scutari, C. Gabbiani, A. Casini, L. Messori, *Coord. Chem. Rev.* 2009, **253**, 1692-1707; b) A. de Almeida, D. E. Oliveira, J. D. G. Correia, G. Soveral, A. Casini, *Coord. Chem. Rev.* 2013, **257**, 2689-2704.
- 17 C. K. Mirabelli, D. T. Hill, L. F. Faucette, F. L. McCabe, G. R. Girard, D. B. Bryan, B. M. Sutton, J. O'Leary Bartus, S. T. Crooke, R. K. Johnson, *J. Med. Chem.* 1987, **30**, 2181-2190.
- 18 CCDC 1045016 (**3ab**), CCDC 1045017 (**3ac**) contain the supplementary crystallographic data for this paper. These data can be obtained free of charge from the Cambridge Crystallographic Data Centre via www.ccdc.cam.ac.uk/data_request/cif.

- 19 PPh₃ and **2b** were tested in the cell lines IGROV1, and HT29. Here, the alkyne proved to be inactive in both cases and the PPh₃ furnished the following IC₅₀ values 47 μM (IGROV1) and 39 μM (HT29).
- 20 C.K. Mirabelli, R.K. Johnson, C.M. Sung, L. Faucette, K. Muirhead and S.T. Crooke, *Cancer Research*, 1985, 45, 32-39.
- 21 I. Mickuviene, V. Kirveliėne, B. Juodka, *Toxicol. In Vitro*, 2004, **18**, 639-648.
- 22 A. Casini, C. [Gabbiani](#), F. [Sorrentino](#), M. P. [Rigobello](#), A. [Bindoli](#), T. J. [Geldbach](#), A. [Marrone](#), N. Re, C. G. [Hartinger](#), P. J. Dyson, L. [Messori L.](#), 2008, *J Med Chem.*, 51, 6773-6781
- 23 K. J. Akerman, A. M. Fagenson, V. Cyril, M. Taylor, M. T. Muller, M. P. Akerman, O. Q. Munro, *J Am Chem Soc.*, 2014, **136**, 5670-82.
- 24 A. Albert, C. Brauckmann, F. Blaske, M. Sperling, C. Engelhard U. Karst, *J. Anal. At. Spectrom.*, 2012, 27, 975-981.